PHOTOSYNTHESIS

A 12 Å carotenoid translocation in a photoswitch associated with cyanobacterial photoprotection

Ryan L. Leverenz,[1]* Markus Sutter,[1,2]* Adjélé Wilson,[3,4] Sayan Gupta,[5] Adrien Thurotte,[3,4] Céline Bourcier de Carbon,[3,4] Christopher J. Petzold,[2] Corie Ralston,[5] François Perreau,[6] Diana Kirilovsky,[3,4] Cheryl A. Kerfeld[1,2,7]†

Pigment-protein and pigment-pigment interactions are of fundamental importance to the light-harvesting and photoprotective functions essential to oxygenic photosynthesis. The orange carotenoid protein (OCP) functions as both a sensor of light and effector of photoprotective energy dissipation in cyanobacteria. We report the atomic-resolution structure of an active form of the OCP consisting of the N-terminal domain and a single noncovalently bound carotenoid pigment. The crystal structure, combined with additional solution-state structural data, reveals that OCP photoactivation is accompanied by a 12 angstrom translocation of the pigment within the protein and a reconfiguration of carotenoid-protein interactions. Our results identify the origin of the photochromic changes in the OCP triggered by light and reveal the structural determinants required for interaction with the light-harvesting antenna during photoprotection.

Photosynthetic organisms balance light harvesting against the toxic effects of oxidative intermediates produced under excess light (*1*). Thermal dissipation of excess absorbed energy—manifested as a quenching of antenna fluorescence known as nonphotochemical quenching (NPQ) (*2*, *3*)—is the predominant photoprotective mechanism. Carotenoid pigments play critical roles in NPQ (*2*–*11*), including a likely role as a direct quencher of excitation energy in "flexible" NPQ mechanisms (*4*) that operate reversibly on short time scales (seconds to minutes) and under dynamic light conditions (*6*–*11*).

In cyanobacteria, a relatively simple carotenoid-dependent NPQ mechanism is associated with the light-harvesting antenna protein complex, the phycobilisome (PB). Here, NPQ is triggered by photoactivation of the soluble orange carotenoid protein (OCP), a blue-light photoreceptor that noncovalently binds a single carotenoid (*3*). Activation of the OCP occurs when its dark (orange) state, OCP^O, absorbs blue light and forms the quenching active (red) state, OCP^R (*12*). OCP^R binds to the PB and initiates PB-associated NPQ (*12*, *13*). Structurally, the OCP is composed of two domains, a mixed α/β C-terminal domain (CTD) and a N-terminal domain (NTD) with an all α-helical fold unique to cyanobacteria (*14*) (fig. S1, A and B). A 4-keto carotenoid (fig. S1C) spans both domains (*14*, *15*) and is almost entirely enclosed by protein (4% solvent-exposed; fig. S1B). The isolated, carotenoid-binding NTD, referred to as the red carotenoid protein (RCP), functions as an effector domain; it binds to PBs and quenches PB fluorescence (*16*). The CTD serves as the regulatory (sensory) domain (*16*, *17*) conferring photochemical activity to the OCP and providing the site of interaction with the fluorescence recovery protein (FRP), which catalyzes the OCP^R-to-OCP^O conversion (*18*). In the absence of the CTD, the RCP is a constitutively active quencher; its activity and spectroscopic properties are essentially identical to those of OCP^R (*16*). However, dissociation or absence of the CTD would leave nearly half of the carotenoid accessible to solvent. This raises a fundamental question about how the hydrophobic carotenoid is structurally accommodated in OCP^R and RCP prior to interaction with the PB.

To probe the molecular details of carotenoid-protein interactions in RCP/OCP^R, we produced RCP by expressing a synthetic *rcp* gene [encoding residues 20 to 165 of *Synechocystis* PCC6803 (hereafter *Synechocystis*) OCP] in echinenone (ECN)– or canthaxanthin (CAN)–producing *E. coli* strains. In both strains, the OCP binds a mixture of CAN and ECN, with a higher relative amount of CAN binding in the CAN-producing strain (table S1). RCP_{CAN} (binding exclusively CAN) was more active than RCP_{ECN} (binding exclusively ECN) and induced PB fluorescence quenching comparable to that of RCP obtained by partial proteolysis (*16*) of the OCP purified from *Synechocystis* (fig. S2). Accordingly, we structurally characterized RCP_{CAN} and its cognate OCP.

The 1.90 Å resolution structure of *Synechocystis* OCP^O_{CAN} (table S2) aligns closely with the structure of *Synechocystis* OCP_{ECN} (*19*) [root mean square deviation (RMSD) 0.17 Å over 304 α-carbon atom pairs]. The carotenoid conformation is also consistent with previously reported OCP^O structures binding ECN (*19*) or hydroxyechinenone (*14*) (table S3), and there is well-defined electron density for each CAN carbonyl oxygen (Fig. 1A and fig. S4A). The OCP_{CAN} was photoactive and able to induce

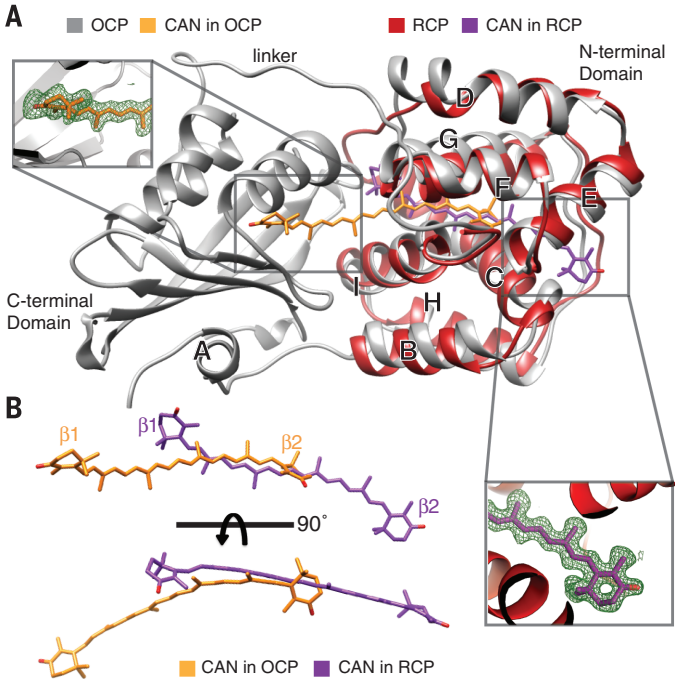

Fig. 1. Crystal structures of the orange carotenoid protein (OCP) and red carotenoid protein (RCP) binding canthaxanthin (CAN). (**A**) Superimposed ribbon structures of OCP_{CAN} (gray) and RCP_{CAN} (red). CAN is shown in orange sticks in OCP, purple sticks in RCP. Inset panels show representative electron density for the carotenoid in each structure (complete carotenoid $F_{obs} - F_{calc}$ maps are shown in fig. S4). (**B**) CAN structures in OCP and RCP show increased planarity of the polyene chain in RCP and distinctly different β-ring configurations.

[1]MSU-DOE Plant Research Laboratory, Michigan State University, East Lansing, MI 48824, USA. [2]Physical Biosciences Division, Lawrence Berkeley National Laboratory, Berkeley, CA 94720, USA. [3]Commissariat à l'Energie Atomique (CEA), Institut de Biologie et Technologies de Saclay (iBiTec-S), 91191 Gif-sur-Yvette, France. [4]Centre National de la Recherche Scientifique (CNRS), I2BC, UMR 9198, 91191 Gif-sur-Yvette, France. [5]Berkeley Center for Structural Biology, Physical Biosciences Division, Lawrence Berkeley National Laboratory, Berkeley, CA 94720, USA. [6]INRA, Institut Jean-Pierre Bourgin, UMR 1318, ERL CNRS 3559, Saclay Plant Sciences, RD10, F-78026 Versailles, France. [7]Department of Plant and Microbial Biology, University of California, Berkeley, CA 94720, USA.
*These authors contributed equally to this work. †Corresponding author. E-mail: ckerfeld@lbl.gov

PB fluorescence quenching (fig. S3). Moreover, the nearly identical UV-visible absorbance spectra for RCP_{CAN} and $OCP^{R}{}_{CAN}$ (fig. S2) indicates that the pigment-protein environments are comparable in $OCP^{R}{}_{CAN}$ and RCP_{CAN}, as reported for the *Arthrospira* homologs (*16*), substantiating their structural and functional homology.

We also determined the RCP_{CAN} structure to 1.54 Å resolution (table S2). The protein backbone of the RCP superimposes on the NTD of $OCP^{O}{}_{CAN}$ (Fig. 1A), with a RMSD of 1.24 Å (104 α-carbon pairs), indicating that large protein conformational changes in the NTD are not involved in PB binding or quenching. However, there is a remarkable difference in the position and conformation of the carotenoid in RCP in comparison to $OCP^{O}{}_{CAN}$. In the active form, the carotenoid is translocated more than 12 Å deeper into the NTD (Fig. 1, A and B). Due to the burrowing of the carotenoid into the NTD, it is only sparingly solvent-accessible (8% solvent-exposed) in RCP, specifically in the vicinity of the two terminal β-ionone rings (β1 and β2, Fig. 1B, Fig. 2A, and fig. S4). Each ring adopts different configurations about the C6-C7 (C6´-C7´) single bond in the two structures (Fig. 1B and Fig. 2A) and the out-of-plane torsions of each ring are decreased relative to those of CAN in OCP^{O} (table S3). The polyene chain is completely encompassed by protein; it assumes a highly planar conformation in RCP, whereas it is bowed and twisted in OCP^{O} (Fig. 1B and fig. S4). The increased planarity of the polyene and reduced β-ring torsions observed for CAN in RCP are consistent with previously published electronic absorption and Raman spectroscopy data that indicate extended effective π-conjugation and a planar all-trans configuration for the carotenoid in both quenching-active RCP and OCP^{R} (*12*, *16*).

The large displacement of the carotenoid has profound consequences for its interactions with the protein. Specifically, the amino acids comprising the CAN binding pockets in the OCP^{O} and RCP structures (Fig. 2A and table S4) occupy two distinct carotenoid-protein configurations (cpcs). In cpcO

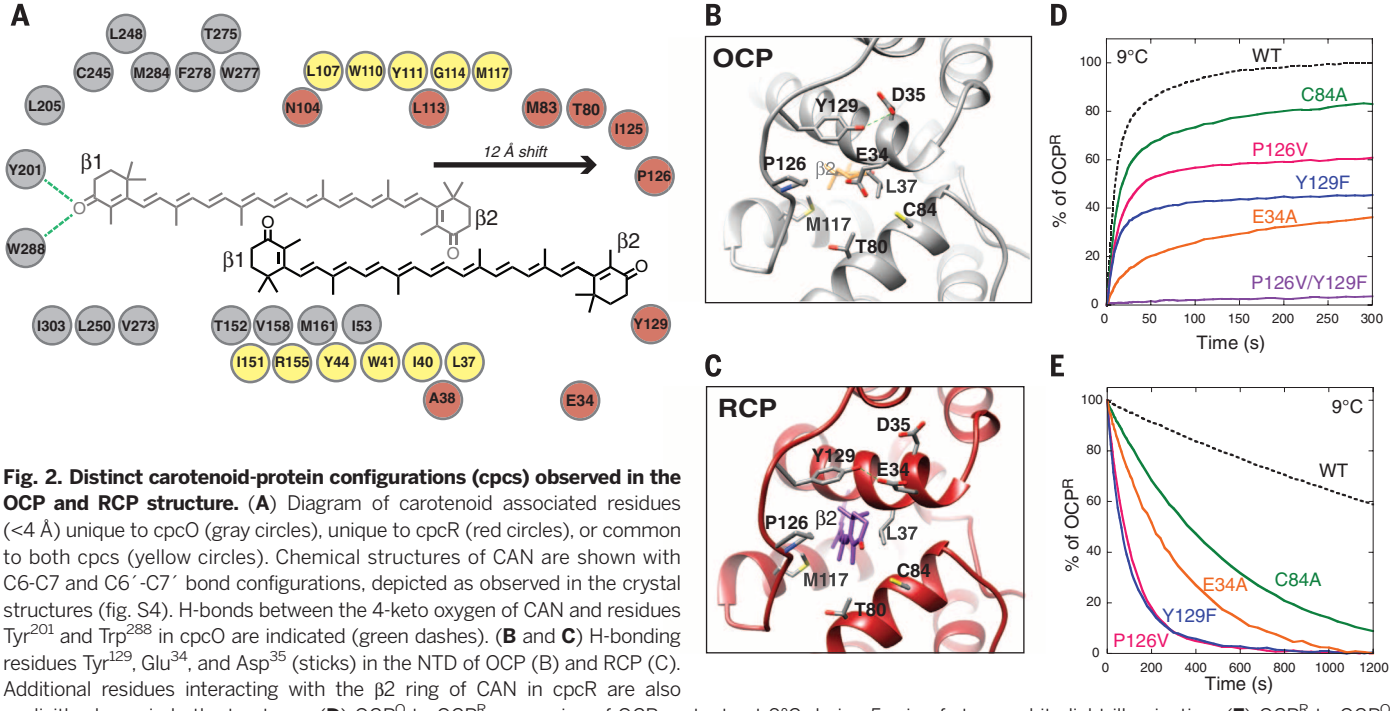

Fig. 2. Distinct carotenoid-protein configurations (cpcs) observed in the OCP and RCP structure. (**A**) Diagram of carotenoid associated residues (<4 Å) unique to cpcO (gray circles), unique to cpcR (red circles), or common to both cpcs (yellow circles). Chemical structures of CAN are shown with C6-C7 and C6´-C7´ bond configurations, depicted as observed in the crystal structures (fig. S4). H-bonds between the 4-keto oxygen of CAN and residues Tyr^{201} and Trp^{288} in cpcO are indicated (green dashes). (**B** and **C**) H-bonding residues Tyr^{129}, Glu^{34}, and Asp^{35} (sticks) in the NTD of OCP (B) and RCP (C). Additional residues interacting with the β2 ring of CAN in cpcR are also explicitly shown in both structures. (**D**) OCP^{O}-to-OCP^{R} conversion of OCP mutants at 9°C during 5 min of strong white-light illumination. (**E**) OCP^{R}-to-OCP^{O} dark recovery at 9°C for mutants in (D).

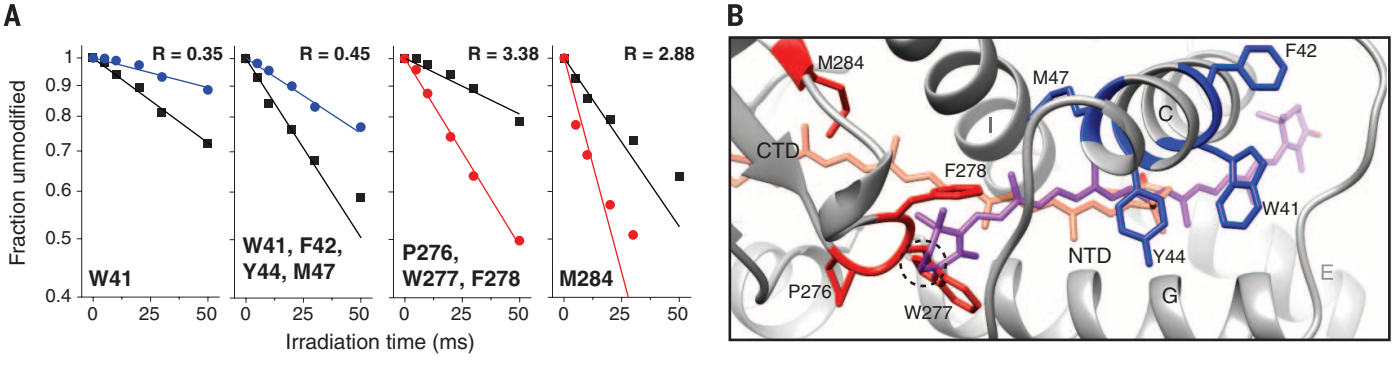

Fig. 3. Solvent accessibility changes in OCP_{CAN} as measured by x-ray hydroxyl radical footprinting. (**A**) Peptide modification as a function of x-ray irradiation dose for Trp^{41}, residue clusters Trp^{41}-Phe^{42}-Tyr^{44}-Met^{47} and Pro^{276}-Trp^{277}-Phe^{278}, and Met^{284} for dark-adapted (OCP^{O}, squares) and illuminated (OCP^{R}, circles) OCP_{CAN}. Solid lines represent single-exponential fits to the dose-dependent data. The ratio of the modification rates (R) indicates the change in relative SA. (**B**) Structural view (OCP_{CAN} structure) of CAN binding residues undergoing large (factor of >2) SA changes after illumination. CAN in cpcO (orange sticks) and CAN in cpcR (purple sticks) are both shown. CTD residues Pro^{276}, Trp^{277}, Phe^{278}, and Met^{284} (red sticks) exhibit a SA increase (R = 3.38, R = 2.88) in OCP^{R}, whereas residue Trp^{41} and residue cluster Trp^{41}-Phe^{42}-Tyr^{44}-Met^{47} (blue) exhibit SA decreases (R = 0.35, R = 0.45). A clash between $Trp^{277}$and CAN in cpcR is indicated (black circle).

(corresponding to CAN in OCP^O), 11 residues of the NTD are in close (<4 Å) proximity to the carotenoid. Retrospectively, the hydrophobic tunnel for translocation of the carotenoid further into the NTD is present in OCP^O (fig. S1B and fig. S5). In cpcR (CAN in RCP) an additional nine residues in this NTD "tunnel" interact with the carotenoid (Fig. 2A). Modest side chain conformational changes accompany translocation (Fig. 2B and fig. S5A). A perturbed local electrostatic environment for CAN in cpcR versus cpcO (fig. S5D), in addition to new H-bonding interactions between solvent and CAN's 4-keto groups in cpcR, likely contribute to altered photophysical properties of the carotenoid (i.e., stabilization of an intramolecular charge transfer state) that may be connected to quenching function (*20*).

The conservation of residues unique to cpcR observed in genes encoding for full-length OCPs (figs. S6 and S7) implicate the carotenoid shift as an integral part of OCP function. Several of the conserved residues within 4 Å of CAN in cpcR were probed by mutagenesis in the OCP. For certain mutations (i.e., $Glu^{34} \rightarrow$ Ala), the CAN:ECN binding ratio was observed to change markedly relative to the wild-type OCP (table S1), indicating that these residues influence carotenoid binding specificity in OCP. The OCP single mutants $Cys^{84} \rightarrow$ Ala, $Tyr^{129} \rightarrow$ Phe, $Pro^{126} \rightarrow$ Val, and $Glu^{34} \rightarrow$ Ala reduced the stability of the OCP^R form, as evidenced by decreased steady-state accumulation of OCP^R after illumination and accelerated OCP^R-to-OCP^O dark-reversion (Fig. 2, D and E); these mutants induced less than 40% PB quenching (fig. S8B). The OCP double mutant $Pro^{126} \rightarrow$ Val/$Tyr^{129} \rightarrow$ Phe remained orange even under prolonged, strong illumination (Fig. 2D and fig. S8), which suggests that these exposed residues, relatively distant from the carotenoid in cpcO, play a critical role in OCP photochemistry. Collectively, these results implicate the CAN-binding residues in cpcR (as observed in the RCP structure) in the stabilization of the carotenoid in the active OCP^R.

To obtain solution-state structural evidence for carotenoid translocation in the OCP^O-to-OCP^R photoconversion, we used x-ray hydroxyl radical footprinting mass spectrometry (XF-MS) to identify changes in side-chain solvent accessibility after illumination (*21*). X-ray dose response plots show that some of the largest solvent accessibility changes after photoconversion occurred in CAN binding residues (Fig. 3A and table S5). The largest solvent accessibility decreases are for peptides containing the NTD residue Trp^{41} (Fig. 3A). The decrease in solvent accessibility for this residue is consistent with an increased interaction with CAN due to CAN translocation. XF-MS analysis of RCP samples exhibited a similarly prominent SA decrease at Trp^{41} (table S5). Furthermore, CTD residues (Pro^{276}-Trp^{277}-Phe^{278} and Met^{284} in OCP^R; Fig. 3A) that contact the CAN polyene chain in cpcO (table S4) had a large increase in solvent accessibility. CAN translocation exposes these side chains to a solvent accessible region in the surface cleft between the CTD and NTD (fig. S1B). Correlated solvent accessibility changes in CAN binding CTD residues (increased solvent accessibility) and NTD residues (decreased solvent accessibility) support carotenoid translocation during OCP activation (Fig. 3B). XF-MS data also confirms that CAN translocation accompanies a separation of the CTD and NTD: The factor of 10 solvent accessibility increase in Arg^{155} (table S5) supports the proposed breakage of the Arg^{155}-Glu^{244} salt bridge in OCP^R (*17*, *22*).

Based on the observation of carotenoid translocation accompanying domain dissociation we propose the following sequence of events in the photoactivation of the OCP (Fig. 4A). Light absorption triggers structural changes in the carotenoid, perturbing its interaction with the CTD (e.g., perturbing H-bonds with Tyr^{201}/Trp^{288}). Light-induced displacement of the N-terminal αA helix from the CTD, proposed to occur based on structtural similarities to the Per-Arnt-Sim family of photosensors (*19*, *23*), has recently been demonstrated by chemical footprinting experiments (*17*). Analogous to the photochemical mechanism of PYP (*24*), it is possible that partial "ejection" of the carotenoid chromophore, driven by a transient, strained cis-carotenoid geometry may be coupled to CTD structural changes. An accompanying reorganization of side chain–pigment interactions has the net effect of destabilizing carotenoid binding in cpcO; translocation of the carotenoid drives the reconfiguration to cpcR. Chaotrope-induced formation of an activated state of the OCP suggests that the transition to cpcR can take place in the absence of light (*25*), implying that translocation may be largely driven by protein-carotenoid binding free energies. In contrast to cpcO, where the carotenoid serves as a structural element bridging the CTD and NTD, carotenoid translocation coupled with dissociation of the αA helix from the CTD (*17*) is required for full domain separation in OCP^R.

The separation of the NTD and CTD in OCP^R leads to solvent exposure of both CAN β rings. The regions surrounding the solvent-exposed β rings (β1, face 1; β2, face 2) include the two largest patches of conserved residues on the surface of RCP (fig. S7). Positive potential, in part due to the critical PB binding residue Arg^{155} (*22*), dominates face 1, whereas face 2 is relatively negatively charged (Fig. 4B). The distinct differences in surface charge between face 1 and face 2 suggest an electrostatically driven directionality in the NTD-PB interaction. Because the conformation of the NTD is essentially unchanged in the active form of the OCP, NTD-PB binding is likely tied to selective exposure of regions of the NTD occluded in OCP^O (face 1 and Arg^{155}), or to the carotenoid translocation itself.

NTD-PB interaction in the vicinity of the exposed β-ring would also be expected for carotenoid-dependent energy quenching, given the importance of interpigment distances in energy transfer efficiency (*26*). Although the atomic-resolution structure of the fully assembled PB is

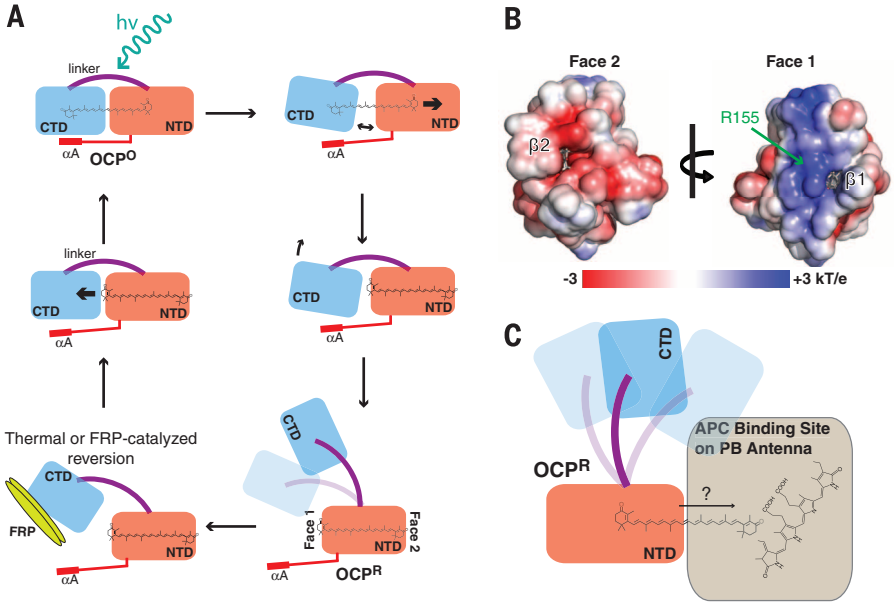

Fig. 4. Proposed models for OCP photoactivation and the site of OCP/RCP-phycobilisome interactions. (**A**) Proposed mechanism for OCP photochemistry, including carotenoid translocation, after light absorption by OCP^O (top left). Structural changes after absorption are localized primarily to the CTD (i.e., dissociation of the αA helix) and are coupled to the translocation (right). Translocation precedes complete NTD-CTD dissociation in OCP^R (bottom right). OCP^R reverts to OCP^O in darkness (thermal reversion) or when catalyzed by an interaction between the fluorescence recovery protein (FRP) and the CTD (*18*) (bottom left); subsequent protein refolding and carotenoid translocation into the CTD (middle left) restores the OCP^O ground state. (**B**) Electrostatic surface potential mapped on the RCP molecular surface colored from red to blue (−3 to +3 *kT/e*). (**C**) OCP:PB interaction illustrating binding at face 1 and a hypothetical carotenoid translocation after binding.

unknown, in silico docking simulations between RCP and PB subunits implicated in OCP-binding (*27*–*29*) show reduced bilin-carotenoid distances as compared to identical simulations with OCP^O (fig. S9A); RCP-PB complexes with face 1 CAN-bilin distances as low as 3.1 Å were identified (fig. S9B). Such close interaction would permit participation of the carotenoid in either direct bilin-carotenoid energy transfer (*20*) or charge transfer quenching mechanisms (*30*). The translocation observed concomitant with activation of the protein raises the possibility of additional carotenoid structural changes and/or movement after binding to the PB (Fig. 4C) to further reduce carotenoid-bilin distances or change the relative orientations of pigments in the OCP-PB complex. More broadly, the light-driven change in carotenoid-protein interactions observed in the OCP prompts a re-examination of other carotenoid binding protein complexes for the possibility of transient, activation-dependent movement of the non-covalently bound carotenoids in those systems.

REFERENCES AND NOTES

1. R. Croce, H. van Amerongen, *Nat. Chem. Biol.* **10**, 492–501 (2014).
2. P. Horton, A. V. Ruban, R. G. Walters, *Plant Physiol.* **106**, 415–420 (1994).
3. D. Kirilovsky, *Photosynth. Res.* **93**, 7–16 (2007).
4. K. K. Niyogi, T. B. Truong, *Curr. Opin. Plant Biol.* **16**, 307–314 (2013).
5. A. A. Pascal *et al.*, *Nature* **436**, 134–137 (2005).
6. H. Staleva *et al.*, *Nat. Chem. Biol.* **11**, 287–291 (2015).
7. H. A. Frank *et al.*, *Photosynth. Res.* **41**, 389–395 (1994).
8. T. K. Ahn *et al.*, *Science* **320**, 794–797 (2008).
9. A. V. Ruban *et al.*, *Nature* **450**, 575–578 (2007).
10. S. Bode *et al.*, *Proc. Natl. Acad. Sci. U.S.A.* **106**, 12311–12316 (2009).
11. P. J. Walla, C.-P. Holleboom, G. R. Fleming, in *Non-Photochemical Quenching and Energy Dissipation in Plants, Algae and Cyanobacteria*, B. Demmig-Adams, G. Garab, W. A. III, Govindjee, Eds. (Springer, Amsterdam, 2014), pp. 229–243.
12. A. Wilson *et al.*, *Proc. Natl. Acad. Sci. U.S.A.* **105**, 12075–12080 (2008).
13. M. Gwizdala, A. Wilson, D. Kirilovsky, *Plant Cell* **23**, 2631–2643 (2011).
14. C. A. Kerfeld *et al.*, *Structure* **11**, 55–65 (2003).
15. C. Punginelli, A. Wilson, J.-M. Routaboul, D. Kirilovsky, *Biochim. Biophys. Acta Bioenerg.* **1787**, 280–288 (2009).
16. R. L. Leverenz *et al.*, *Plant Cell* **26**, 426–437 (2014).
17. H. Liu *et al.*, *Biochim. Biophys. Acta Bioenerg.* **1837**, 1955–1963 (2014).
18. M. Sutter *et al.*, *Proc. Natl. Acad. Sci. U.S.A.* **110**, 10022–10027 (2013).
19. A. Wilson *et al.*, *J. Biol. Chem.* **285**, 18364–18375 (2010).
20. R. Berera *et al.*, *J. Phys. Chem. B* **116**, 2568–2574 (2012).
21. S. Gupta, R. D'Mello, M. R. Chance, *Proc. Natl. Acad. Sci. U.S.A.* **109**, 14882–14887 (2012).
22. A. Wilson *et al.*, *Plant Cell* **24**, 1972–1983 (2012).
23. C. A. Kerfeld, M. Alexandre, D. Kirilovsky, in *Carotenoids: Physical, Chemical and Biological Functions and Properties*, J.T. Landrum, Ed. (CRC Press, Boca Raton, FL, 2009), pp. 3–17.
24. U. K. Genick *et al.*, *Science* **275**, 1471–1475 (1997).
25. J. D. King, H. Liu, G. He, G. S. Orf, R. E. Blankenship, *FEBS Lett.* **588**, 4561–4565 (2014).
26. G. D. Scholes, K. P. Ghiggino, *J. Phys. Chem.* **98**, 4580–4590 (1994).
27. D. Jallet, M. Gwizdala, D. Kirilovsky, *Biochim. Biophys. Acta Bioenerg.* **1817**, 1418–1427 (2012).
28. D. Jallet *et al.*, *Plant Physiol.* **164**, 790–804 (2014).
29. H. Zhang *et al.*, *Biochemistry* **53**, 13–19 (2014).
30. L. Tian *et al.*, *J. Am. Chem. Soc.* **133**, 18304–18311 (2011).

ACKNOWLEDGMENTS

Supported by the U.S. Department of Energy (DOE), Basic Energy Sciences, award DE-FG02-91ER20021. We thank the staff at the Berkeley Center for Structural Biology, which is supported in part by the National Institute of General Medical Sciences and the Howard Hughes Medical Institute. We thank R. Celestre for assistance at beamline 5.3.1. The Advanced Light Source at Lawrence Berkeley National Laboratory is supported by the Office of Science, Office of Basic Energy Sciences, of the U.S. DOE under contract no. DE-AC02-05CH11231. This research used resources of the National Energy Research Scientific Computing Center, a DOE Office of Science User Facility supported by the Office of Science of the U.S. DOE under contract no. DE-AC02-05CH11231 and of the Joint BioEnergy Institute supported by the Office of Science, Office of Biological and Environmental Research, of the U.S. DOE under contract DE-AC02-05CH11231. A.W., A.T., C.B., and D.K. are supported by a grant from the Agence Nationale de la Recherche (ANR, project CYANOPROTECT), and used resources of CNRS and the Commissariat à l'Energie Atomique (CEA). We thank S. Cot for technical assistance. Coordinates have been deposited in the RCSB Protein Data Bank under accession codes 4XB4 (RCP_{CAN}) and 4XB5 (OCP_{CAN}).

SUPPLEMENTARY MATERIALS

www.sciencemag.org/content/348/6242/1463/suppl/DC1
Materials and Methods
Figs. S1 to S9
Tables S1 to S6
References (*31*–*47*)

19 January 2015; accepted 8 May 2015
10.1126/science.aaa7234

MARINE SULFUR CYCLE

Identification of the algal dimethyl sulfide–releasing enzyme: A missing link in the marine sulfur cycle

Uria Alcolombri,[1,2] Shifra Ben-Dor,[3] Ester Feldmesser,[4] Yishai Levin,[4] Dan S. Tawfik,[1]* Assaf Vardi[2]*

Algal blooms produce large amounts of dimethyl sulfide (DMS), a volatile with a diverse signaling role in marine food webs that is emitted to the atmosphere, where it can affect cloud formation. The algal enzymes responsible for forming DMS from dimethylsulfoniopropionate (DMSP) remain unidentified despite their critical role in the global sulfur cycle. We identified and characterized Alma1, a DMSP lyase from the bloom-forming algae *Emiliania huxleyi*. Alma1 is a tetrameric, redox-sensitive enzyme of the aspartate racemase superfamily. Recombinant Alma1 exhibits biochemical features identical to the DMSP lyase in *E. huxleyi*, and DMS released by various *E. huxleyi* isolates correlates with their Alma1 levels. Sequence homology searches suggest that *Alma1* represents a gene family present in major, globally distributed phytoplankton taxa and in other marine organisms.

Dimethylsulfoniopropionate (DMSP) is the major precursor of atmospheric dimethyl sulfide (DMS) and a key component of the ocean sulfur cycle. DMSP has been proposed to have physiological roles as an intracellular osmolyte and antioxidant (*1*) and also serves as an infochemical in interspecies predator-prey interactions, symbiosis, and pathogenicity (*2*–*5*). The volatile DMS is generated in oceans at remarkably high amounts, $>10^7$ tons per year. It is emitted to the atmosphere (*6*) by enzymes known as DMSP lyases and has a global role in atmosphere-ocean feedback processes (*7*, *8*). DMS also serves as a chemoattractant for phytoplankton, bacteria, zooplankton, fish, and sea birds (*3*, *9*, *10*). Several candidate DMSP lyases have been identified in marine bacteria (*11*, *12*); however, the identification of the algal DMSP lyase(s) is crucial for understanding the physiological roles of DMS, its oceanic origins, and the marine sulfur cycle (*12*–*14*) (Fig. 1).

We undertook a classical biochemical fractionation approach combined with shotgun proteomics to identify the DMSP lyase from *Emiliania huxleyi*. This coccolithophore algae is a well-established ecological model organism that forms massive oceanic blooms (*15*, *16*) and has high DMSP lyase activity (*17*). We based our search on two natural *E. huxleyi* isolates: NCMA373, which has a high level of DMSP lyase activity (*17*) (~10 fmol $cell^{-1}$ min^{-1}; herein, HL373), and NCMA374, which shows traces of activity (~2×10^{-3} fmol $cell^{-1}$ min^{-1}; LL374). Despite the different activity levels, both isolates have similar concentrations of intracellular DMSP (*17*).

Nearly all activity observed in the crude HL373 cell lysate was associated with the membrane fraction of the chloroplast and was retained by a 100-kD filter, indicating a relatively large enzyme or complex (fig. S1) [see the supplementary materials (SM)]. Because previous studies suggested antioxidant roles for DMSP and DMS (*1*) and

[1]Department of Biological Chemistry, Weizmann Institute of Science, Rehovot 76100, Israel. [2]Department of Plant and Environmental Sciences, Weizmann Institute of Science, Rehovot 76100, Israel. [3]Bioinformatics and Biological Computing Unit, Biological Services, Weizmann Institute of Science, Rehovot 76100, Israel. [4]Nancy and Stephen Grand Israel National Center for Personalized Medicine, Weizmann Institute of Science, Rehovot 76100, Israel.
*Corresponding authors. E-mail: assaf.vardi@weizmann.ac.il (A.V.); dan.tawfik@weizmann.ac.il (D.S.T.)

Science

A 12 Å carotenoid translocation in a photoswitch associated with cyanobacterial photoprotection

Ryan L. Leverenz, Markus Sutter, Adjélé Wilson, Sayan Gupta, Adrien Thurotte, Céline Bourcier de Carbon, Christopher J. Petzold, Corie Ralston, François Perreau, Diana Kirilovsky and Cheryl A. Kerfeld

Science **348** (6242), 1463-1466.
DOI: 10.1126/science.aaa7234

Protection from too much light

Photosynthetic organisms protect themselves from too much light using pigment photoswitches that absorb excess energy. Leverenz *et al.* analyzed the structure of an active, energy-dissipating form of the orange carotenoid protein (OCP) from a cyanobacterium. When activated by excess light, OCP moves its hydrophobic carotenoid pigment 12 Å within the protein to accommodate nonphotochemical quenching by the broader photosynthetic antenna complex.

Science, this issue p. 1463